# Pattern formation in growth of snow crystals occurring in the surface kinetic process and the diffusion process

Etsuro Yokoyama and Toshio Kuroda
*The Institute of Low Temperature Science, Hokkaido University, Sapporo 060, Japan*
(Received 19 June 1989)

We propose a model of pattern formation in the growth of snow crystals that takes into account the actual elemental processes relevant to the growth of crystals, i.e., a surface kinetic process for incorporating molecules into a crystal lattice and a diffusion process. This model gives a clear correspondence between the patterns produced and the actual growth conditions such as supersaturation and the diffusion coefficient. Circular patterns due to kinetic roughening, hexagonal patterns, and dendritic patterns are obtained starting from a circular crystal under various growth conditions. We analyze these patterns and discuss the mechanisms of appearance of round patterns, the development of hexagonal patterns, and the formation of dendritic patterns of snow crystals. Finally, it is shown that the dimensionless crystal size with reference to the mean free path of a water molecule plays an important role in the pattern formation of growing snow crystals.

## I. INTRODUCTION

The great variety of growth forms of snow crystals is one of the marvels of nature. The form of a growing snow crystal changes with time as follows. First, a spherical single ice crystal of the order of $1-10$ $\mu$m in radius is formed by the freezing of a supercooled water droplet in a cloud; this frozen droplet adsorbs supersaturated water vapor, thus growing into a hexagonal prism, which is the fundamental form of ice crystals bounded by two basal $\{0001\}$, and six prism $\{10\bar{1}0\}$, faces.[1,2] The hexagonal prism develops further into various patterns such as plate, column, needle, sector plate, and dendrite according to the growth conditions in the cloud.[3,4] Since the growth rate of each position of a surface depends on growth conditions, the pattern produced therefore depends on those conditions.

Nakaya investigated for the first time the relation between the growth patterns of snow crystals and the growth conditions of temperature $T$ and supersaturation $\sigma$ with respect to ice.[5] Since then many experimental studies of growth patterns have been made.[6-8] These results are consolidated in a $(T,\sigma)$ diagram by Kobayashi[8] (Fig. 1).

This diagram first shows that the complicated habit change of snow crystals occurs with a decrease in temperature; i.e., the plates change to columns at $T=-4\,^{\circ}$C, columns change to plates at $-10\,^{\circ}$C, and plates change to columns at $-22\,^{\circ}$C. It has recently been found that the habit change depending on temperature is attributable to surface melting and the roughening of basal and prism faces.[9,10] The diagram shows secondly that the morphological instability of polyhedral crystals occurs with an increase in the degree of supersaturation. At low supersaturation polyhedral snow crystals can grow in a stable way, retaining their forms. With increasing supersaturation, however, their patterns develop into sector plates and, where supersaturation is high, into dendrites at $T=-15\,^{\circ}$C or into needles at $T=-6\,^{\circ}$C by preferred growth of edges and corners of the crystal; this is morphological instability.[11,12]

Here we should distinguish this instability from the Mullikins-Sekerka instability for the round interface, e.g., the crystal-melt interface, which is rough in the molecular scale.[13,14] In the latter case, the dendrites develop from perturbations at the interface. Furthermore, equilibrium conditions are assumed at the interface, since the kinetic barrier for the growth of the rough interface is negligible.

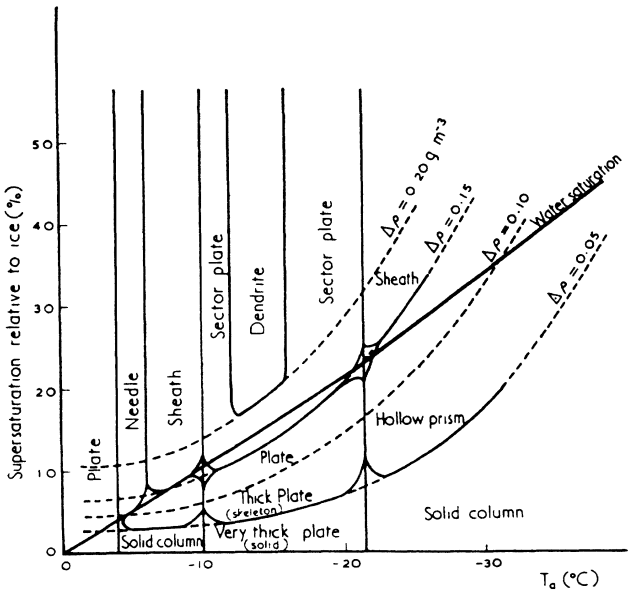


FIG. 1. Habit changes and stability of polyhedral forms of snow crystals depending on temperature and supersaturation with respect to ice [after Kobayashi (Ref. 8)].

 

The growth patterns of snow crystals also depend on factors other than temperature and supersaturation. It has been found that the development of skeletal or dendritic structures is reduced by an increase in the diffusion coefficient of water vapor, and, on the other hand, the development of these structures increases with increasing thermal conductivity of the atmosphere.[15–18]

However, theoretical studies on the time evolution of the pattern of growth have recently been developed. There are the following two approaches.

The first is an approach which assumes simple growth laws and produces various complicated patterns similar to natural snow dendrites.[19–22] The second is an approach which takes into account actual elemental processes relevant to the growth of crystals; these are the surface kinetic process for incorporating water molecules into a crystal lattice and the diffusion process.[23]

Although the former approaches, using simple growth laws, seem to have succeeded, they are unsatisfactory as regards the correspondence to the actual growth processes of snow crystals. Specifically, it is impossible to clarify the quantitative relation between the parameters appearing in the simple growth laws and the actual growth conditions given by supersaturation, diffusion coefficient, and so on. Recently, in order to obtain this correspondence, a Monte Carlo simulation based on a modified diffusion-limited-aggregation (DLA) model[24] with a simplified surface kinetic process has been carried out.[25] However, the quantitative consideration of the mechanism of pattern formation of growth represented by Fig. 1 still remains insufficient. Therefore the second approach mentioned above is significant for obtaining a clear correspondence between the patterns produced and the actual growth conditions, even though it involves a mathematically difficult treatment.

The actual elemental processes relevant to the growth of snow crystals are as follows: (i) a diffusion process for supplying water molecules in air toward the crystal surface, (ii) a surface kinetic process for the incorporation of water molecules into the ice crystal lattice, which includes their adsorption onto a crystal surface; surface diffusion of admolecules toward the steps, which are supplied by two-dimensional nucleation or with the aid of screw dislocations; and the lateral motion of the steps, etc.; and (iii) a heat conduction process for removing the latent heat generated at the crystal surface.

It is quite obvious that these processes are closely reflected in growth patterns of snow crystals. In particular, the surface kinetic process plays a very important role in the formation of such polyhedral features of snow crystals as hexagonal prisms and facets seen at the tips of dendrites (Fig. 2). We emphasize that such surfaces are molecularly smooth and that they cannot grow without the lateral motion of steps. However, in the previous theoretical studies of pattern formation only the diffusion process was considered and the surface kinetic process was completely disregarded,[26–28] since the rough surface is tacitly assumed in their papers. As a result, the tips of dendrites produced are round and their methods never produce facets.

The purposes of the present study are as follows: (i) to produce the growth patterns of snow crystals under various growth conditions such as supersaturation and the diffusion coefficient by computer simulation which takes into account the diffusion process and the surface kinetic process, (ii) to analyze the patterns produced by the simulation, and (iii) to discuss the mechanisms of the appearance of round pattern, the development of facets, and the formation of a dendritic pattern in terms of both processes.

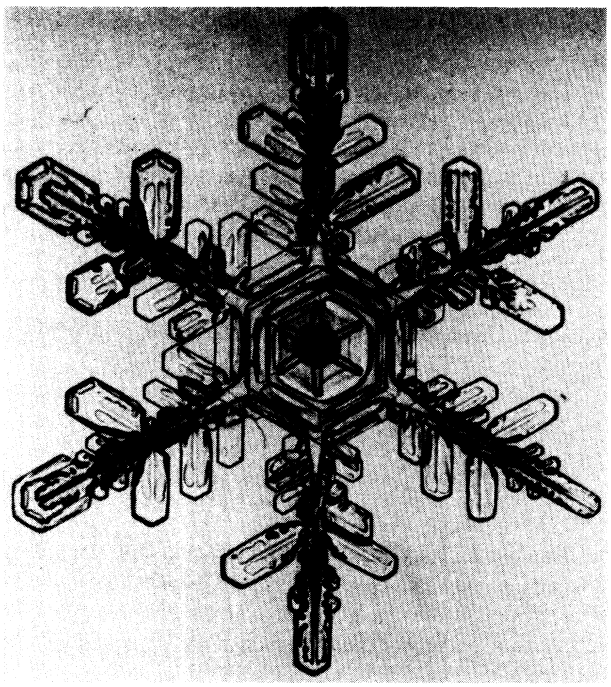

FIG. 2. A typical example of snow crystals (provided by Furukawa).

To be precise, the heat conduction process may also contribute to the pattern formation of snow crystals. However, it can be considered that its contribution to the growth rate is relatively small compared to the diffusion and the surface kinetic processes, unless the growth rate is too large.[29,30] Furthermore, it has been found experimentally that the heat conduction process contributes minimally to the pattern formation.[17]

This moving boundary problem in which two processes are coupled is extremely difficult to solve. To simplify the problem, we treat two-dimensional single crystals starting from a circle which is perpendicular to the $c$ axis of a hexagonal snow crystal. This boundary value problem is solved by means of the boundary element method (BEM).[23] Then the growth under the conditions of no air flow is treated. The effect of air flow on pattern formation will be discussed briefly in Sec. III. Lastly, the temperature of the whole system is assumed to be uniform at $-15\,^{\circ}\mathrm{C}$, which is a typical temperature for the development of dendritic pattern crystals.

## II. GROWTH PROCESSES AND METHODS OF SIMULATION

### A. Surface kinetic process

Figure 3 shows part of a growing crystal surface composed of a number of monomolecular steps. The growth rate $V_k$ determined by a surface kinetic process in the direction normal to a surface is given by

$$V_k=\beta(\theta,\sigma_s)\sigma_s \ , \tag{1}$$

where $\sigma_s$ is the local surface supersaturation and $\beta(\theta,\sigma_s)$ is the kinetic coefficient.

$\sigma_s$ is defined using the pressure $p_s$ of the water vapor at the surface and the equilibrium vapor pressure $p_e$ of ice

$$\sigma_s=\frac{p_s-p_e}{p_e} \ . \tag{2}$$

For the kinetic barrier to be overcome, the degree of slight excess vapor pressure $p_s-p_e$ or supersaturation $\sigma_s$ at the surface should be positive. Thus $\sigma_s$, i.e., the driving force for surface kinetic process, is included in the growth rate $V_k$.

$\beta(\theta,\sigma_s)$ represents the activity of the surface for incorporating the water molecules into the crystal lattice. The surface inclined by $\theta$ from the singular surface, i.e., a molecularly smooth surface, grows by the lateral motion of steps which are, in a parallel manner, distributed with a distance $\lambda$ corresponding to $\theta$. Thus the surface grows by $d$ when the steps advance by $\lambda$. Burton, Cabrera, and Frank[31] obtained the rate of advancement of a step by solving the two-dimensional surface diffusion equation of admolecules in which the molecular flux from the vapor to the terraces is taken into account. As a result, the $\beta(\theta,\sigma_s)$ is expressed as

$$\beta(\theta,\sigma_s)=\beta_{\max}\frac{s}{s_1}\tanh\frac{s_1}{s} \ , \tag{3}$$

$$s=\tan\theta=d/\lambda \ , \tag{4}$$

$$s_1=d/2x_s \ , \tag{5}$$

$$\beta_{\max}=\alpha_1 v_c p_e/(2\pi mkT)^{1/2} \ , \tag{6}$$

where $\lambda$ is the mean step distance, $d$ the step height, $x_s$ the mean surface diffusion distance of a molecule on the surface, $\alpha_1$ the sticking coefficient, i.e., the ratio of molecules that stick on the surface at the instant when they have impinged on it, $v_c$ the volume of a molecule in the crystal, $m$ the mass of a molecule, $k$ the Boltzmann constant, and $T$ the absolute temperature. It should be noticed that $\beta(\theta,\sigma_s)$ depends not only on the local slope $s=\tan\theta$ of the surface against the singular surface but also on $\sigma_s$ through the frequency of generation of steps on the singular surface and their lateral motion.

Figure 4 shows the dependence of $\beta(\theta,\sigma_s)$ on $\theta$, which is, schematically, the rotation angle about the $c$ axis. It possesses six minimums at 0°, ±60°, ±120°, and 180° corresponding to six prism faces, i.e., singular surfaces which are smooth on a molecular level. Although there is no step on the prism faces in the equilibrium state, the steps are actually generated by two-dimensional nucleation or with the aid of screw dislocation in the nonequilibrium state. As shown with thick arrows in Fig. 4, the kinetic coefficient $\beta_0=\beta(0,\sigma_s)$ of prism faces is not zero but positive. The value is determined by the slope $s_0=\tan\theta_h$ of a growth hillock composed of generated steps on the prism face. It is to be noted that the development of facets is due to anisotropy of $\beta(\theta,\sigma_s)$. Since the frequency of step generation increases in keeping with $\sigma_s$, the slope $s_0$ formed by steps increases in keeping with $\sigma_s$. The anisotropy of $\beta(\theta,\sigma_s)$ is weakened with increasing $\beta_0$, which is determined by $\sigma_s$ on prism faces. If $\beta_0$ becomes equal to $\beta_{\max}$ with an increase in $\sigma_s$, the anisotropy of $\beta(\theta,\sigma_s)$ completely vanishes. We call a vanishment of anisotropy of growth rate due to such kinetic reason the kinetic roughening.

In the case of spiral growth with the aid of a screw dislocation,[31,32] the slope $s_0=\tan\theta_h$ of a growth hillock on prism faces is given by

$$s_0=\frac{d}{19r^*}\simeq\frac{d\sigma_s}{2x_s\sigma_1} \ , \tag{7}$$

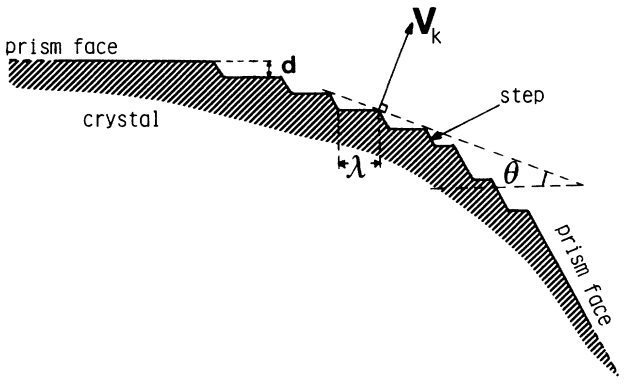


FIG. 3. Schematic representation of the step distribution of a growing crystal surface.

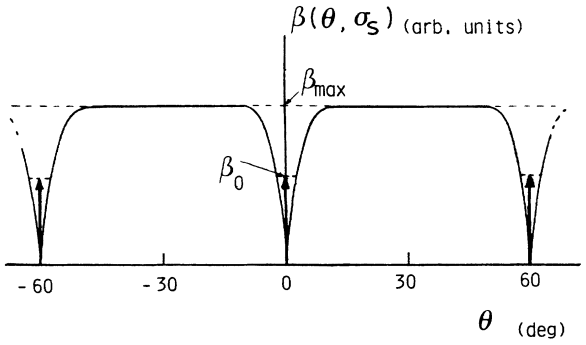


FIG. 4. Dependence of the kinetic coefficient $\beta(\theta,\sigma_s)$ on $\theta=\tan^{-1}s$, which is the rotation angle about the $c$ axis.

$$\sigma_1=\frac{9.5f_0\kappa}{kTx_s}\ , \tag{8}$$

where $r^*$ is the radius of a critical two-dimensional nucleus, $\kappa$ the edge free energy per unit length along a step, and $f_0$ the surface area occupied by a molecule.

The kinetic coefficient $\beta_0=\beta(0,\sigma_s)$ for spiral growth increases linearly with $\sigma_s$ in the range of $\sigma_s \ll \sigma_1$, since the frequency of step generation increases with increasing $\sigma_s$, and approaches $\beta_{\max}$ for $\sigma_s \gg \sigma_1$ [Fig. 5(a)], because neighboring steps scramble for admolecules when $\sigma_s$ exceeds $\sigma_1$. When we assign the edge free energy $\kappa=2.0\times10^{-6}$ erg/cm,[33] the growth rates obtained by Eqs. (1)–(8) agree well with experimental values[34] [Fig. 5(b)].

In order to interpret the experimental values by two-dimensional nucleation growth,[35] we must assign an extraordinarily small value $\kappa=4.0\times10^{-7}$ erg/cm.[33] On the other hand, the value of the edge free energy derived from the broken bond model is very large,[9] i.e., $\kappa=3.7\times10^{-6}$ erg/cm. Although the actual value may be smaller because of the entropy effect and adsorption of impurities at the step, $\kappa=4.0\times10^{-7}$ erg/cm assigned for the two-dimensional nucleation growth, this value is unreasonably smaller than the value for the broken bond model. Accordingly, we consider only the spiral growth to occur with the aid of a screw dislocation and assign $\kappa=2.0\times10^{-6}$ erg/cm. Furthermore, the steps are supplied from screw dislocations emerging at the center of six prism faces until a circular crystal develops into a perfect hexagon, and they are generated at its corners where the supersaturation is largest, once a perfect hexagon has been developed.

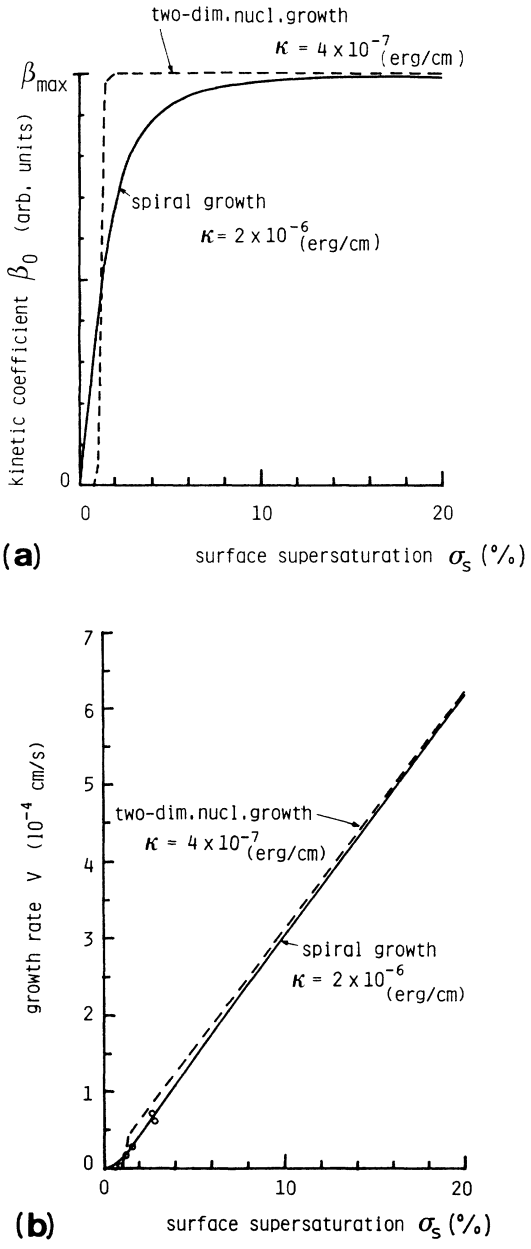


FIG. 5. (a) Dependence of the kinetic coefficient $\beta_0$ for prism faces on the surface supersaturation $\sigma_s$ in the case of spiral growth for edge free energy $\kappa=2.0\times10^{-6}$ erg/cm (solid line) and in the case of two-dimensional growth for edge free energy $\kappa=4.0\times10^{-7}$ erg/cm (dashed line). (b) Dependence of the growth rate $V$ on the surface supersaturation $\sigma_s$ corresponding to (a) for spiral growth (solid line) and for two-dimensional growth (dashed line). Open circles show the experimental values in Ref. 34.

### B. Diffusion process

Using the typical growth rate of snow crystals and the diffusion coefficient of water molecules, it can be shown that the growth rate of the crystal surface is negligibly small in comparison with the quick movement of the molecules by diffusion. Accordingly, the supersaturation $\sigma$ in the region $\Omega$ surrounding a crystal (Fig. 6) is governed by the quasistatic diffusion equation

$$\Delta\sigma=0\ . \tag{9}$$

The boundary conditions for solving Eq. (9) are as follows: (i) the supersaturation is specified by

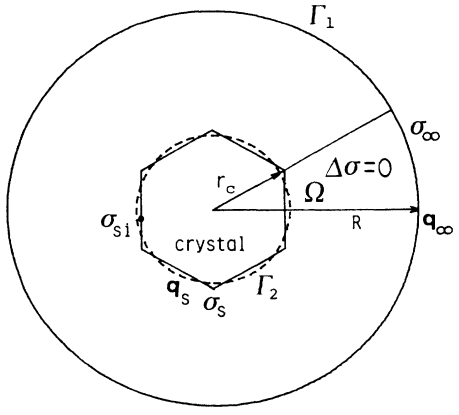


FIG. 6. Diffusion field surrounding a crystal.

$$\sigma=\sigma_\infty \tag{10}$$

on the boundary $\Gamma_1$ which is set off the center of the crystal by the distance $R$, and (ii) mass conservation condition is required on the boundary $\Gamma_2$ representing the crystal surface, i.e., the growth rate $V_k$ determined by the surface kinetic process should be equal to the growth rate $V_d$ determined by the volume diffusion process under steady-state conditions[11,12]

$$V_k=V_d=V\ . \tag{11}$$

The growth rate $V_k$ is given by Eq. (1) and the growth rate $V_d$ is given by

$$V_d=\frac{v_c p_e}{kT}Dq_s\ , \tag{12}$$

where $D$ is the diffusion coefficient and $q_s=(\partial\sigma/\partial n)_s$ the normal gradient of supersaturation at a position on the surface. Thus, by substituting Eqs. (1) and (12) into Eq. (11), we obtain the boundary conditions on $\Gamma_2$ as follows:

$$\beta(\theta,\sigma_s)\sigma_s-\frac{v_c p_e}{kT}Dq_s=0\ . \tag{11'}$$

Equation (11') is important for determining self-consistently the growth rate $V$ controlled both by the diffusion process and by the surface kinetic process.

This problem, characterized by the boundary conditions Eq. (11') involving both $\sigma_s$ and its derivative $q_s$, is a so-called third boundary value problem which remains unclarified. It should be noted that both distributions $\sigma_s$ and $q_s$ are unknown, but they are connected by Eq. (11').

### C. Methods of simulation

We solve Eq. (9) by means of the boundary element method as follows.[23] At first, we obtain the boundary integral equation from Eq. (9) using Green's theorem and boundary conditions [Eqs. (10) and (11')]:

$$\sigma_{si}/2+\int_{\text{along }\Gamma_2}\left[q^*+\sigma^*\frac{kT\beta(\theta,\sigma_s)}{v_c p_e D}\right]\sigma_s d\Gamma = \int_{\text{along }\Gamma_1}(q_\infty\sigma^*-\sigma_\infty q^*)d\Gamma\ , \tag{13}$$

where $\sigma_{si}$ is the supersaturation at a point $i$ on $\Gamma_2$ representing the crystal surface (Fig. 5), $q_\infty$ the normal gradient of supersaturation on $\Gamma_1$ which is set off the center of the crystal by the distance $R$, $\sigma^*$ satisfies $\Delta\sigma^*+\delta_i=0$ ($\delta_i$, the Dirac delta function at a point $i$), and $q^*$ is $\partial\sigma^*/\partial n$. We approximately replace $q_\infty$ with the following equation under the assumption that $\Gamma_1$ is far from $\Gamma_2$:

$$q_\infty=\frac{\sigma_\infty}{R\ln(R/r_c)}\ , \tag{14}$$

which is obtained for the diffusion field surrounding a circular crystal with a radius $r_c$, which is half of the mean length along the $a$ and $b$ axes and with a perfect sink, i.e., $\sigma_s=0$.

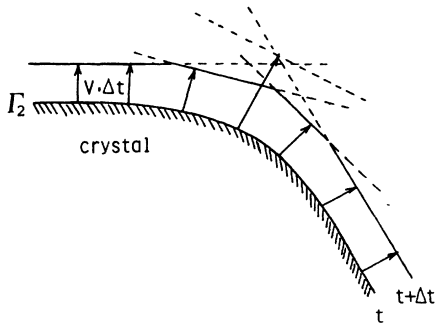


FIG. 7. Procedure for drawing a growth pattern.

$\Gamma_2$ is divided into $N$ elements, Eq. (13) is changed to an algebraic equation with respect to the surface supersaturation $\sigma_s$, and $N$ simultaneous equations for all points $i$ are derived from the algebraic equation. We find the distribution of $\sigma_s$ by solving these algebraic equations and, consequently, get the growth rate $V$ at each position on the surface at a certain moment and then determine the shape of a growing surface after $\Delta t$ sec. Here, the value of $\beta(\theta,\sigma_s)$ in Eq. (13) is determined by only the local slope $s=\tan\theta$ except $\beta_0$ at the prism faces. On the other hand, the $\beta_0$ depends on $\sigma_s$ through the slope of the growth hillock [Eq. (7)]. $\beta_0$ and $\sigma_s$, therefore, must be self-consistently solved by iteration methods.[12] To avoid calculation errors, the number $N$ of elements is so increased in keeping with the crystal periphery that the length of each element is kept nearly constant.

It is to be noted that the faster growing surface is cut by neighboring slower growing surfaces, while the slowest growing surface develops the largest area. A growth pattern is, therefore, determined by the inner envelope of the lines perpendicular to each vector $V\Delta t$ at its point because of the finite value $\Delta t$ (Fig. 7). By repeating this procedure we can simulate the pattern formation in the growth of snow crystals.

## III. RESULTS

The numerical values used for simulation are as follows: temperature $T=281.15$ K ($=-15$ °C), equilibrium vapor pressure $p_e=1.66\times10^3$ dyn/cm$^2$$=1.66\times10^2$ Pa corresponding to $-15$ °C, molecular volume of ice crystal $v_c=3.25\times10^{-23}$ cm$^3$, surface area occupied by a water molecule $f_0=8.3\times10^{-16}$ cm$^2$, mass of a water molecule $m=3.0\times10^{-23}$ g, step height or lattice constant $d=4.5\times10^{-8}$ cm, mean surface diffusion distance of an admolecule $x_s=400d$,[36] adsorption energy $E_{ad}=6.23\times10^{-13}$ erg/molecule,[36] Boltzmann constant $k=1.38\times10^{-16}$ erg/deg, edge free energy per unit length along a step $\kappa=2.0\times10^{-6}$ erg/cm (see Sec. II), radius of initial crystal $r_{c0}=5\times10^{-3}$ cm, ratio of a distance $R$ to the outer boundary $\Gamma_1$ from the crystal to an average radius $r_c$ of the crystal (Fig. 6) $R/r_c=6.5$—when this ratio is used, the growth rate in this two-dimensional simulation is nearly equal to that of the three-dimensional model, i.e., spherical crystal.

### A. Development of facets and kinetic roughening

Figures 8, 9, and 10 show three examples of pattern formation for large diffusion coefficient $D=40$ cm$^2$/s (corresponding to 500 Pa of air pressure, i.e., about $5\times10^{-3}$ atm) and the sticking coefficient[37,38] $\alpha_1=0.1$ at various supersaturations $\sigma_\infty$. Since water molecules are supplied to the crystal surface faster at large $D$, the supersaturation $\sigma_s$ at the surface does not largely drop from $\sigma_\infty$.

For the sake of convenience let us define the degree of anisotropy of the kinetic coefficient as

$$\delta\beta=\frac{\beta_{\max}-\beta_0}{\beta_{\max}}, \tag{15}$$

where $\delta\beta=1$ means the maximum anisotropy which corresponds to the limit of $\sigma_s\to0$, and $\delta\beta=0$ means complete vanishment of anisotropy. It is to be noted that $\delta\beta$ increases with a decrease in surface supersaturation $\sigma_s$, since the value of $\beta_0$ for prism faces decreases in keeping with its surface supersaturation $\sigma_s$. Figure 8 shows

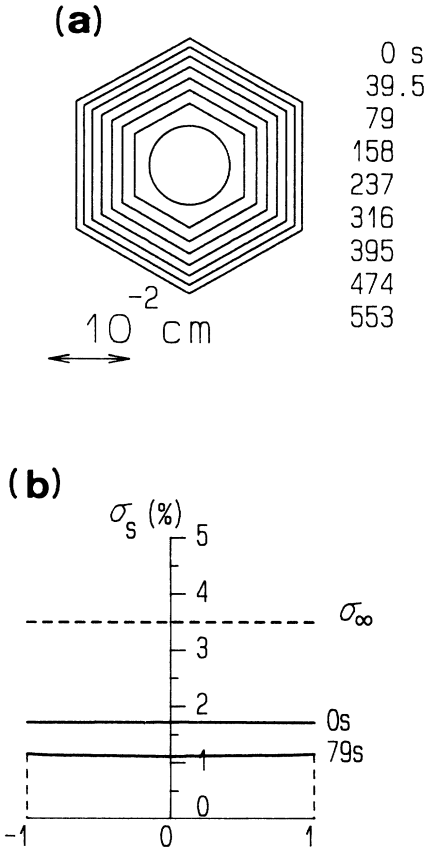


FIG. 8. (a) Development of prism faces, i.e., hexagonal pattern for $D=40$ cm$^2$/s (corresponding to 500 Pa of air pressure) and $\sigma_\infty=3.5\%$. (b) Supersaturation along the crystal surface. The degree of anisotropy $\delta\beta=0.4$ at 0 s. $\sigma_s(1)=1.26\%$ at corners denoted by $\pm1$, $\sigma_s(0)=1.23\%$ at centers of surface denoted by 0 at 79 s.

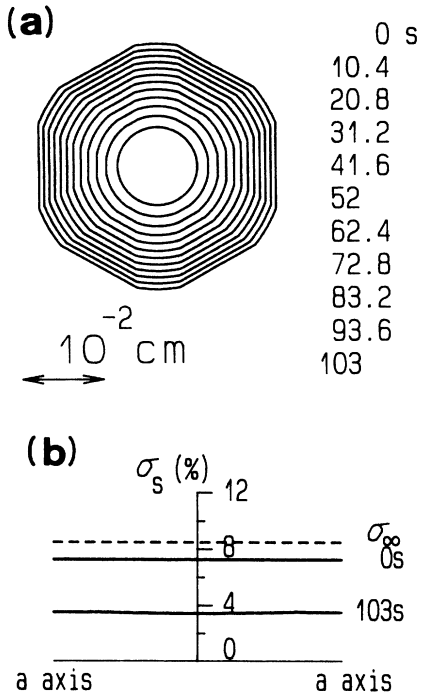


FIG. 9. (a) Development of prism facets due to the recovery of the anisotropy of the growth rate with increasing surface area for $D=40$ cm$^2$/s and $\sigma_\infty=8.5\%$. (b) $\delta\beta=0.04$ at 0 s.

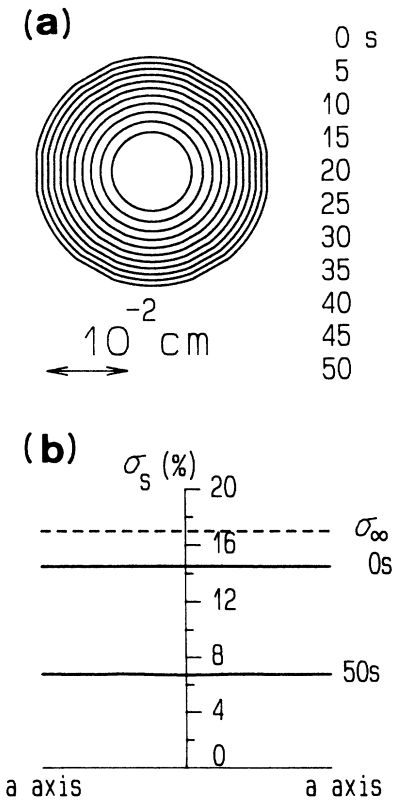


FIG. 10. (a) Circular pattern due to kinetic roughening for $D=40$ cm$^2$/s and $\sigma_\infty=17\%$. (b) $\delta\beta=0.01$ at 0 s; $\delta\beta=0.04$ at 50 s.

$\delta\beta=0.4$ at 0 s. The surface supersaturation $\sigma_s$ is small for $\sigma_\infty=3.5\%$ in spite of large $D$. Consequently, prism faces develop their area easily and an initial circular crystal becomes a perfect hexagon within 79 s, since anisotropy of the kinetic coefficient is large. Then, the hexagonal crystal grows retaining its flat surface.

Since the supersaturation $\sigma_s$ at the surface increases consistently with $\sigma_\infty$, the anisotropy of the kinetic coefficient $\delta\beta$ decreases with an increase in $\sigma_\infty$. In Fig. 9 ($\sigma_\infty=8.5\%$), $\delta\beta=0.04$ at 0 s. This value is one-tenth of $\delta\beta$ in Fig. 8 ($\sigma_\infty=3.5\%$) at 0 s, so that an initial circular crystal cannot develop into a perfect hexagon even when the crystal size has increased to three times the initial size.

Furthermore, the $\sigma_s$ increases as $\sigma_\infty$ increases in Fig. 10. Hence, the anisotropy of the kinetic coefficient decreases extremely with increasing $\sigma_\infty$. Since $\delta\beta=0.01$ at 0 s because of larger $\sigma_\infty=17\%$ in Fig. 10, the anisotropy of the growth rate almost vanishes. In other words, a so-called kinetic roughening defined in Sec. II occurs. Accordingly, the prism faces can hardly develop, even though the crystal size increases to three times the initial size during growth for 50 s. Furthermore, Fig. 10 also shows that small facets begin to develop as the crystal grows further. This is due to a decrease in $\sigma_s$ with increasing crystal size, since the supply of water molecules to the surface becomes insufficient because of the increase in the area of surface acting as sink for molecules. In fact, $\delta\beta$ increases to 0.04 at 50 s, in keeping with crystal size [Fig. 10(b)].

Figure 11 shows an example for small $D=0.2$ cm$^2$/s (corresponding to 1 atm, i.e., $1.013\,25\times10^5$ Pa) and $\alpha_1=0.01$ (Ref. 38) at $\sigma_\infty=8.5\%$. Since $\sigma_s$ largely drops from $\sigma_\infty$ because of the insufficient supply of molecules by diffusion under the conditions of small $D$, $\delta\beta$ is larger in comparison with the case of $D=40$ cm$^2$/s. For example, $\delta\beta=0.74$ at 0 s in Fig. 11. This value is much larger than $\delta\beta=0.04$ at 0 s in Fig. 9. Hence, the prism faces can grow easily, as shown in Fig. 11, and an initial circular crystal becomes a perfect hexagon during a slight growth in size.

The growth rate is much smaller than that for $D=40$ cm$^2$/s (compare growth times in Fig. 9 with those in Fig. 11), since $\sigma_s$ in Fig. 11(b) is smaller than that in Fig. 9(b). Furthermore, the supersaturation is not uniform over its surface[39] at 1200 s: it is largest $\sigma_s(1)=0.73\%$ at the corners denoted with $\pm1$ and smallest $\sigma_s(0)=0.56\%$ at the center of the surface denoted by 0. Let us define the degree of inhomogeneity in supersaturation as

$$\delta\sigma=\frac{\Delta\sigma}{\sigma_s(1)}\ , \tag{16}$$

where $\Delta\sigma=\sigma_s(1)-\sigma_s(0)$. Since $\delta\sigma$ in Fig. 11(b) ($=0.23$ at 1200 s) is not large enough for preferred growth of corners, the hexagonal crystal grows retaining its flat surface in spite of its inhomogeneity. The details will be described in Sec. IV.

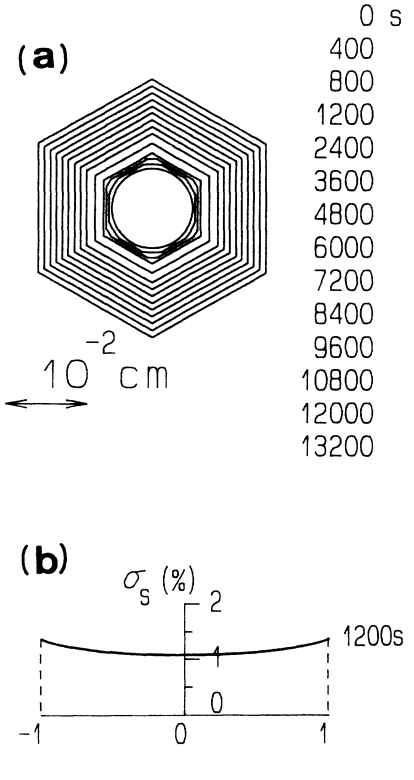


FIG. 11. (a) Hexagonal pattern for $D=0.2$ cm$^2$/s (corresponding to 1 atm) and $\sigma_\infty=8.5\%$. (b) $\sigma_s(1)=0.73\%$, $\sigma_s(0)=0.56\%$, and $\delta\sigma=0.23$ at 1200 s.

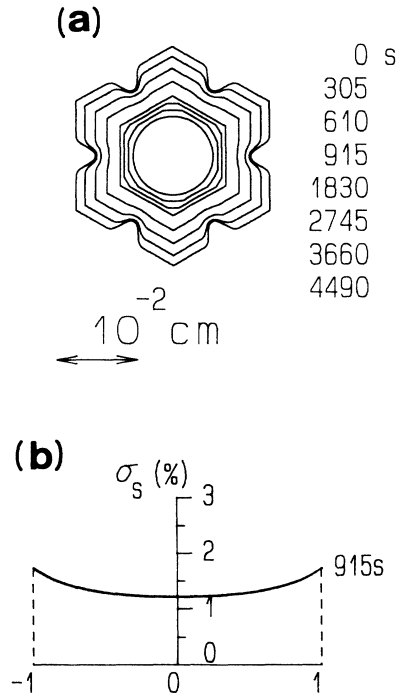


FIG. 12. (a) Dendritic pattern for $D=0.2$ cm$^2$/s and $\sigma_\infty=17\%$. (b) $\sigma_s(1)=1.73\%$, $\sigma_s(0)=1.22\%$, and $\delta\sigma=0.29$ at 915 s.

### B. Dendritic pattern

Figures 12–14 show examples of dendritic pattern for small $D=0.2$ cm$^2$/s and $\alpha_1=0.01$ at various $\sigma_\infty$. The degrees of anisotropy at 0 s are as follows: $\delta\beta=0.51$ in Fig. 12, $\delta\beta=0.34$ in Fig. 13, and $\delta\beta=0.12$ in Fig. 14.

When an initial circular crystal has become a perfect hexagon in Fig. 12, the growth rate at the corners is larger than that at the center of the surface because of the large inhomogeneity in surface supersaturation, and consequently preferred growth at the corners begins. This is the onset of transition from a hexagonal to a dendritic pattern. Figure 12(b) shows that the supersaturation inhomogeneity is $\delta\sigma=0.29$ at 915 s. This value is greater than that of Fig. 11(b) ($\delta\sigma=0.23$) because of an increase in $\sigma_\infty$.

Furthermore, the dendritic pattern becomes more remarkable and the width of a primary branch decreases with an increase in $\sigma_\infty$ in Figs. 13 and 14. We will discuss the reason in Sec. IV. It should be noted that the dendritic patterns shown in Figs. 13 and 14 are obtained for $\sigma_\infty$ (26% and 50%), much larger than the maximum supersaturation 16% at $-15$ °C, which is realized when water vapor is equilibrated with supercooled water droplets in clouds, while similar patterns are seen in natural snow crystals grown during their fall in clouds at $\sigma_\infty \leq 16\%$. The difference between $\sigma_\infty$ in this simulation and $\sigma_\infty$ in natural growth can be explained as follows. If the air flows relatively to the snow crystal, the thickness $\delta_d$ of a diffusion boundary layer decreases in proportion to $N_{\mathrm{Re}}{}^{-1/2}$ ($N_{\mathrm{Re}}$: the Reynolds number, which is proportional to flow velocity $U$),[40] while $\delta_d$ is of the order of crystal size for $U=0$ in this simulation. On the other hand, $\sigma_s$ increases with decreasing $\delta_d$ for a constant $\sigma_\infty$. When snow crystals grow during their fall through the air under conditions of water saturation, $\sigma_s$ can reach the large value enough for dendritic pattern; for example, 3.69% which corresponds to the growth at $\sigma_\infty=50\%$ in simulation for $U=0$.

Figure 15 shows further development of dendritic pattern for $\sigma_\infty=34\%$. The crystal size is about 0.8 mm across in diameter. One should note that the six primary branches grow with a periodical structure at the tips which is caused by bunching of monomolecular steps. Such bunches may act as the trigger for the formation of secondary branches.

## IV. ANALYSES OF THE PATTERN FORMATION AND DISCUSSION

### A. Kinetic roughening

As defined in Sec. II, the kinetic roughening corresponds to such vanishment of anisotropy of growth rate

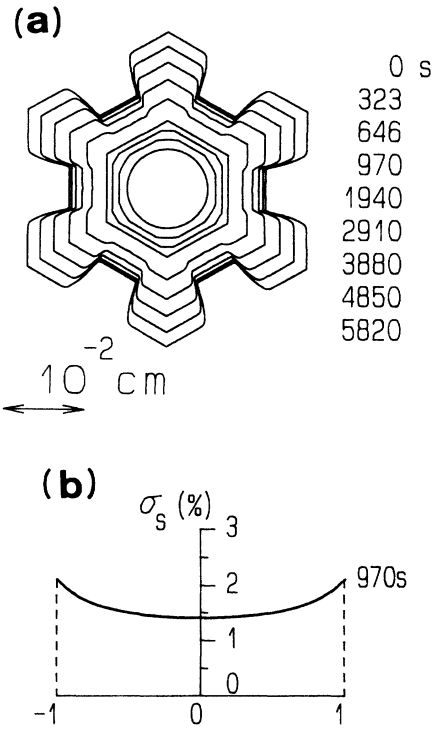


FIG. 13. (a) Dendritic pattern for $D=0.2$ cm$^2$/s and $\sigma_\infty=26\%$. (b) $\sigma_s(1)=2.11\%$, $\sigma_s(0)=1.41\%$, and $\delta\sigma=0.33$ at 970 s.

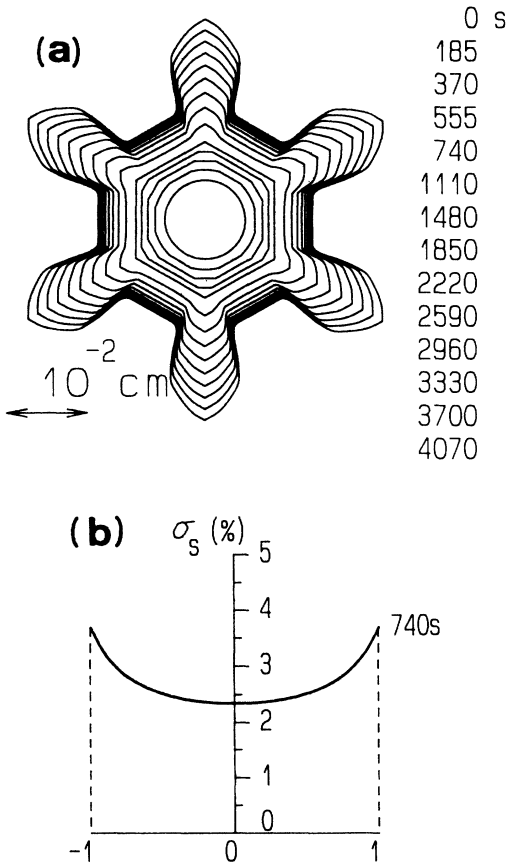


FIG. 14. (a) Dendritic pattern for $D=0.2$ cm$^2$/s and $\sigma_\infty=50\%$. (b) $\sigma_s(1)=3.69\%$, $\sigma_s(0)=2.35\%$, and $\delta\sigma=0.36$ at 740 s.

that the kinetic coefficient $\beta_0$ for prism faces becomes equal to $\beta_{\max}$ with increasing surface supersaturation $\sigma_s$. To be precise, $\beta_0$ reaches $\beta_{\max}$ only when $\sigma_s$ approaches the infinite value. However, a crystal actually becomes spherical on the scale of the optical microscope at large finite $\sigma_s$. Accordingly, let us so define it that the kinetic roughening occurs when

$$\beta_0=\beta_0^*=0.98\beta_{\max} . \tag{17}$$

By substituting Eqs. (3), (5), (7), and (8) into Eq. (17), we obtain the critical surface supersaturation $\sigma_s^*$ above which kinetic roughening occurs

$$\sigma_s^*=53.2\frac{f_0\kappa}{kTx_s} . \tag{18}$$

It is to be noted that $\sigma_s^*$ depends on the step energy $\kappa$. For the numerical values used in this study, $\sigma_s^*=13.8\%$.

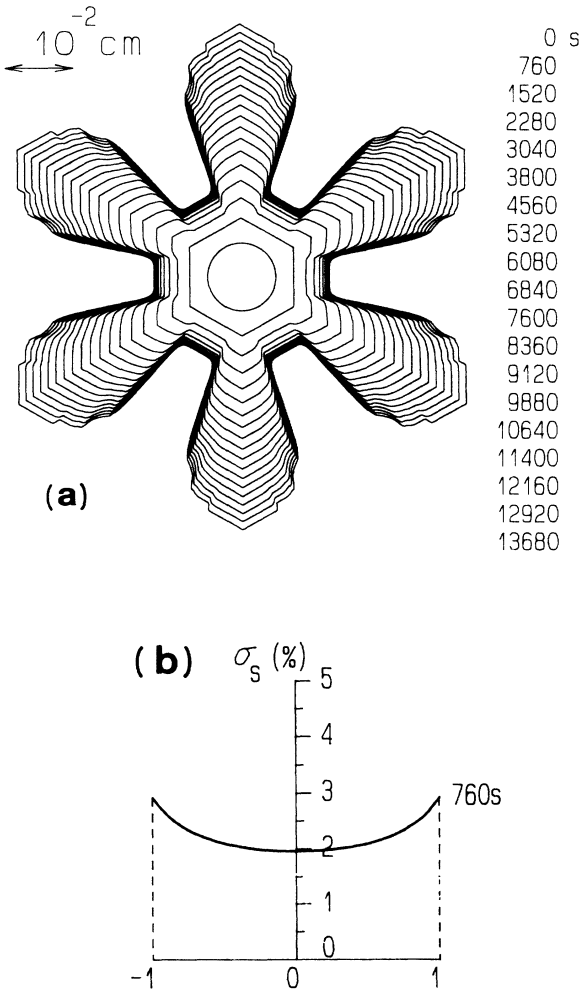


FIG. 15. (a) Dendritic pattern with a periodical structure at the tips for $D=0.2$ cm$^2$/s and $\sigma_\infty=34\%$. (b) $\sigma_s(1)=2.92\%$, $\sigma_s(0)=1.97\%$, and $\delta\sigma=0.33$ at 970 s.

On the other hand, $\sigma_s$ controlled both by the diffusion process and the surface kinetic process depends on the supersaturation $\sigma_\infty$ at infinity, the diffusion coefficient $D$, and crystal size $r_c$. When the kinetic roughening takes place, the supersaturation $\sigma_s=(\sigma_s^*)$ is constant all over the surface of the circular crystal. Hence, from the mass conservation conditions at the surface [Eq. (11')], the following equation is obtained:

$$\beta_{\max}\sigma_s^*=\frac{v_c p_e D}{kT}\frac{\sigma_\infty-\sigma_s^*}{r_c\ln(R/r_c)} . \tag{19}$$

By substituting Eq. (6) into $\beta_{\max}$ in Eq. (19), we obtain

$$\sigma_s^*=\frac{\sigma_\infty}{1+\varkappa_c} , \tag{20}$$

where

$$\varkappa_c=\frac{\alpha_1\bar{v}r_c\ln(R/r_c)}{4D} , \tag{21}$$

and

$$\bar{v}=\left[\frac{8kT}{\pi m}\right]^{1/2} . \tag{22}$$

Here $\bar{v}$ is the mean speed of water molecules. By substituting the value of $\sigma_s^*$ determined by Eq. (18) in Eq. (20), we obtain the relation between $\sigma_\infty$, $D$, and $r_c$ corresponding to critical conditions for the kinetic roughening.

For drawing the relation between $\sigma_\infty$, $D$, and $r_c$ [Eq. (20)] corresponding to critical conditions for the kinetic roughening in the diagram distinguishing between hexagonal and dendritic patterns (Fig. 17), we rewrite $r_c$ in Eq. (21) by $2\pi r_c\ln(R/r_c)=6L$, where $L$ is the length of a side of hexagon. Thus we obtain

$$\sigma_s^*=\frac{\sigma_\infty}{1+6/\Delta\phi\mathcal{L}} , \tag{23}$$

where $\Delta\phi=\phi(\frac{2}{3})-\phi(\frac{1}{2})=0.5554$, $\phi(\frac{2}{3})$, and $\phi(\frac{1}{2})$ are the polygamma function; $\mathcal{L}$ is given by Eq. (28). The relation between $\sigma_\infty$ and $\mathcal{L}$ given by Eq. (23) for $\sigma_s^*=13.8\%$ is represented by a dashed line in Fig. 17.

### B. Mechanism of dendritic pattern formation

When a hexagonal crystal grows retaining its macroscopically flat surface, the supersaturation is not uniform over its surface—it is largest $\sigma_s(1)$ at the corners, and smallest $\sigma_s(0)$ at the center of surface (Fig. 11).

First let us consider the reason why a hexagonal crystal can grow retaining its flat surface in spite of the inhomogeneity in supersaturation for smaller $\sigma_\infty$ (Refs. 11 and 12) (see Fig. 11). The steps generated at the corners where $\sigma_s(1)$ is largest spread toward the center of the surface where $\sigma_s(0)$ is smallest. Since the step velocity reduces approaching the center of the surface because of the decrease in $\sigma_s$ from the corners to the center of the surface, the steps become closer together approaching the center of the surface. As a result, the local slope is smallest at the corners and largest at the center of the surface

(Fig. 16). Since the local kinetic coefficient $\beta$ increases with local slope [Eq. (3)], $\beta$ increases from the corners toward the center of the surface. Thus the growth rate $V(0)$ at the center of the surface can reach $V(1)$ at the corners and the growth rate $V$ can be constant over the whole surface, if the inhomogeneity $\delta\sigma$ in supersaturation is small. It should be noted that the surface of the hexagonal crystal is macroscopically flat, since such small $\delta\sigma$ can be compensated by a slight local slope of the order of $10^{-2}$ at the center of the surface.

On the other hand, the slope at center of the surface increases in keeping with $\sigma_\infty$, since the inhomogeneity $\delta\sigma$ increases with $\sigma_\infty$. Consequently, the value of $\beta$ at the center reaches the value of the upper limit $\beta_{\max}$ with increasing $\sigma_\infty$ because of step-step interaction through surface diffusion of admolecules. Once $\beta$ at center of the surface becomes equal to $\beta_{\max}$ at critical supersaturation $\sigma_\infty^{**}$, the growth rate $V(0)$ at the center of the surface can never reach the growth rate $V(1)$ at the corners at $\sigma_\infty$ above $\sigma_\infty^{**}$, even though the slope at the center of the surface increases in keeping with $\sigma_\infty$. After all, the critical conditions for the limit of stable growth of the hexagonal crystal, i.e., transition from hexagonal to dendritic pattern, is given by,[12]

$$V_{k,\max}(0)^{**}=V_k(1)^{**} ,$$

or

$$\beta_{\max}\sigma_s(0;\sigma_s^{**})=\beta(\sigma_s^{**})\sigma_s^{**} , \tag{24}$$

where $V_{k,\max}(0)^{**}$ is the maximum growth rate corresponding to $\beta_{\max}$ at the center of the surface, $V_k(1)^{**}$ the critical growth rate at the corners, $\sigma_s^{**}=\sigma_s^{**}(1)$ the critical supersaturation at the corners, and $\sigma_s(0;\sigma_s^{**})$ the critical supersaturation at the center of the surface which depends on $\sigma_s(1)^{**}$ [Eqs. (25) and (26)].

Here, in the case of the regular hexagonal crystal, the supersaturation inhomogeneity $\Delta\sigma=\sigma_s(1)-\sigma_s(0)$ is expressed as[39]

$$\Delta\sigma=\frac{\Delta\phi}{2\pi}Lq_s . \tag{25}$$

The normal gradient $q_s$ of the supersaturation at surface is represented by Eq. (11′),

$$q_s=\frac{kT\beta(\sigma_s^{**})}{v_c p_e D}\sigma_s^{**} . \tag{26}$$

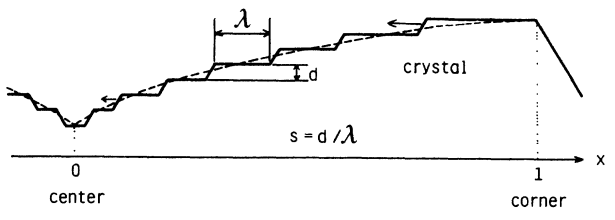


FIG. 16. Schematic representation of the step distribution for compensation of inhomogeneity in supersaturation.

By substituting Eqs. (25) and (26) in Eq. (24) and rearranging the expression, we obtain

$$\frac{\sigma_s^{**}}{\sigma_1}\tanh\frac{\sigma_1}{\sigma_s^{**}}=\frac{1}{1+\mathcal{L}} , \tag{27}$$

where $\mathcal{L}$ is the dimensionless crystal size given as follows:

$$\mathcal{L}=\frac{\Delta\phi}{8\pi}\frac{\alpha_1\bar{v}L}{D} . \tag{28}$$

In Eq. (28), it should be noted that the ratio of diffusion coefficient $D$ to the mean speed of water molecules $\bar{v}$ is the mean free path of a water molecule $\bar{l}$. Thus $\mathcal{L}$ is the dimensionless crystal size with reference to $\bar{l}$.

On the other hand, the surface supersaturation $\sigma_s(1)$ at the corners is determined as a function of the supersaturation $\sigma_\infty$, diffusion coefficient $D$, and crystal size. Let us derive the relation between $\sigma_\infty$, $D$, and $L$ corresponding to the critical conditions that $\sigma_s(1)$ becomes equal to the value $\sigma_s^{**}$ determined by Eq. (27). The $\sigma_s(1)$ is given as[39,41]

$$\sigma_s(1)=\sigma_\infty-\frac{\Delta\phi}{8\pi}FLq_s , \tag{29}$$

where $F$ is a constant which depends on the ratio $R/L$. Here, $R$ is the distance from the crystal to the outer boundary $\Gamma_1$. By substituting Eqs. (26), (27), and (28) in Eq. (29), we obtain the surface supersaturation under the conditions for transition from the hexagonal to the dendritic pattern

$$\sigma_s^{**}=\frac{\sigma_\infty}{1+F\mathcal{L}/(1+\mathcal{L})} . \tag{30}$$

The relation between $\sigma_\infty$, $D$, and $L$ corresponding to the conditions for transition from the hexagonal to the dendritic pattern can be obtained by solving the simultaneous Eqs. (27) and (30).

### C. Diagram of growth pattern

Figure 17 is a diagram showing relation between patterns and conditions $(\sigma_\infty,\mathcal{L})$. The solid line in Fig. 17 represents the transition from the hexagonal to the dendritic pattern determined by Eqs. (27) and (30) for $F=25$ corresponding to $R/r_c=6.5$. The dashed line represents conditions for kinetic roughening given by Eqs. (23) with $\sigma_s^*=13.8\%$.

The diagram clearly shows three regions of patterns, i.e., a circular pattern due to kinetic roughening, a hexagonal pattern, and a dendritic pattern. Furthermore, the diagram also shows that an increase in $\mathcal{L}$ during the growth causes a transition from the circular pattern due to kinetic roughening to hexagonal pattern to dendritic pattern at constant $\sigma_\infty$ above 16%. The dash-dotted line $A$ in Fig. 17 corresponds to the conditions of $D=40$ cm$^2$/s, $\alpha_1=0.1$, and $r_c=50$ $\mu$m. The dash-dotted line $B$ in Fig. 17 corresponds to the conditions $D=0.2$ cm$^2$/s, $\alpha_1=0.01$, and $L=100$ $\mu$m. Under later conditions, the value $\sigma_s^{**}$ for the transition from the hexagonal to the dendritic pattern is nearly equal to 17%. It should be

noted that the produced patterns of snow crystals sensitively depend on $\sigma_\infty$ for the constant $\mathcal{L}$ (Fig. 17).

Let us interpret why the width of a primary branch decreases with an increase in $\sigma_\infty$ in the region of dendritic patterns (Figs. 12–15). The results of simulation mean that the position $x$, where the growth rate can never reach the growth rate $V(1)$ at the corners, moves toward the corner from the center of the surface with increasing $\sigma_\infty$. The $x$, which is normalized by $L/2$, is a temporary measure of the width of a primary branch.

In a way similar to the derivation of conditions for transition from hexagonal to dendritic pattern, $x$ is determined by the conditions $V(x)=V(1)$. Furthermore, we assume that Eqs. (25) and (26) hold at the onset of the formation of dendritic pattern, and obtain

$$\frac{\sigma_s(1)}{\sigma_1}\tanh\frac{\sigma_1}{\sigma_s(1)}=\frac{1}{1+\mathcal{L}(1-x^2)} . \tag{31}$$

In Eq. (31), $x=0$ corresponds to Eq. (27)—the conditions for transition from hexagonal to the dendritic pattern. Since the left-hand side of Eq. (31) increases through $\sigma_s(1)$ in keeping with $\sigma_\infty$, $x$ has to approach 1, i.e. the corners. The width $(1-x)$ of the primary branch, therefore, decreases with an increase in $\sigma_\infty$.

Figure 18 is a three-dimensional ($T$, $\sigma_\infty$, and $\mathcal{L}$) diagram which is composed of both a diagram showing the relation between patterns and conditions $(\sigma_\infty,\mathcal{L})$ at $-15\,^\circ$C (Fig. 17) and a diagram showing the relation between patterns (Fig. 1) seen in snow crystals grown in the growth chamber and conditions $(T,\sigma_\infty)$.[8] It should be noted that the $(T,\sigma_\infty)$ diagram is based on the experiment without convection ($U=0$). The same conditions are set also in this study. Consequently, the transition from plates to sector plates in the $(T,\sigma_\infty)$ diagram occurs

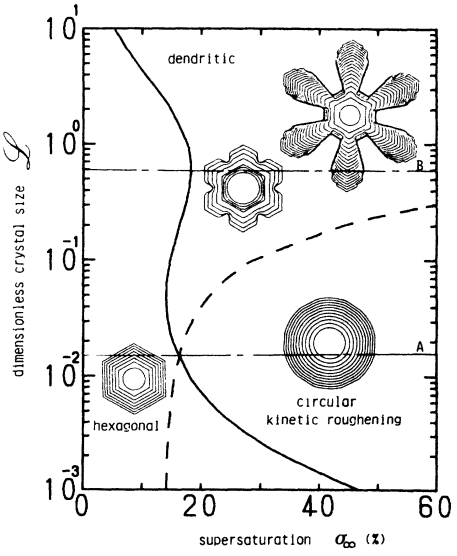


FIG. 17. Diagram showing the relation between the obtained patterns and conditions $(\sigma_\infty,\mathcal{L})$.

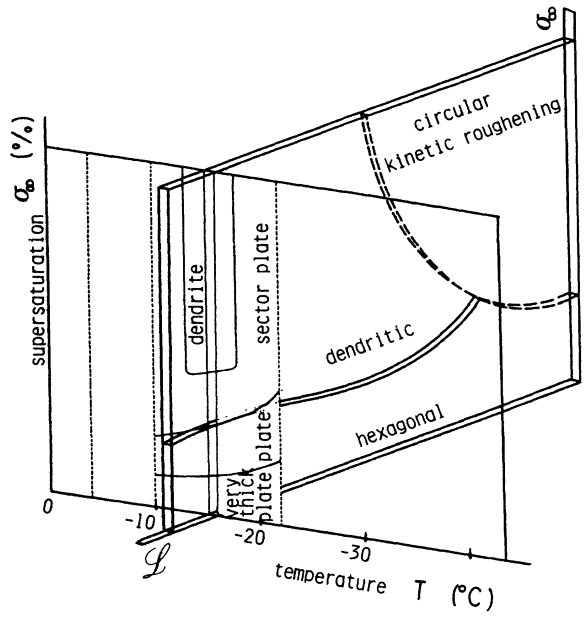


FIG. 18. Three-dimensional ($T,\sigma_\infty$, and $\mathcal{L}$) diagram, which is composed of both Figs. 17 and 1.

near the critical value $\sigma_\infty^{**}$ distinguishing the hexagonal pattern and the dendritic pattern in the range of $10^{-2}>\mathcal{L}>5\times10^{-3}$ (corresponding to the order of crystal size $10^{-1}$ cm in the atmosphere) in the $(\sigma_\infty,\mathcal{L})$ diagram.

It has been considered that the patterns of snow crystals were determined only by the temperature $T$ and the supersaturation $\sigma_\infty$ so far. As shown in Fig. 18, however, the patterns of snow crystals also depend on the dimensionless crystal size $\mathcal{L}$ with reference to the mean free path $\bar{l}(=D/\bar{v})$ of a water molecule [Eq. (28)].

## V. CONCLUDING REMARKS

In the present study, a simulation of the pattern formation of growing snow crystals was carried out by taking into account both the surface kinetic process and the diffusion process. A variety of patterns of snow crystals was produced corresponding to the various growth conditions such as supersaturation and the diffusion coefficient. Then, the features of the patterns were analyzed from the standpoint of not only the growth conditions but also the crystal size, and the mechanisms of formation of the pattern of growing snow crystals were discussed in terms of the diffusion process and the surface kinetic process.

The following three patterns of snow crystals are obtained. (i) Circular pattern due to kinetic roughening: Prism faces can hardly grow because of the vanishment of anisotropy of growth rate, i.e., kinetic roughening, and a circular pattern remains during growth. (ii) Hexagonal pattern: An initial circular crystal develops into the perfect hexagon bounded by six prism faces, and then the hexagonal crystal can grow retaining its flat surface macroscopically. (iii) Dendritic pattern: An initial circu-

lar crystal develops into the perfect hexagon, and then the hexagon develops into a dendritic pattern by way of preferred growth of six corners. The width of a primary branch decreases with an increase in supersaturation.

The critical conditions for kinetic roughening are given by the supersaturation $\sigma_\infty$ and the dimensionless crystal size $\mathcal{L}$. The conditions for the transition from the hexagonal to the dendritic pattern are also given by $\sigma_\infty$ and $\mathcal{L}$. It is shown for the first time that the dimensionless crystal size $\mathcal{L}$ with reference to the mean free path $\bar{l}$ of a water molecule plays an important role in the pattern formation of growing snow crystals. Specifically, the pattern of growing snow crystal depends not only on the temperature and the supersaturation but also on the dimensionless crystal size.

## ACKNOWLEDGMENTS

We wish to express gratitude to Professor Y. Suzuki of the Institute of Low Temperature Science (ILTS), Hokkaido University; and Professor K. Kikuchi of the Department of Geophysics, Hokkaido University, for helpful discussions. We wish to thank Dr. Y. Furukawa, of ILTS for providing a photograph of snow crystals. We are also grateful to Mr. T. Irisawa, of the Department of Physics, Gakushuin University, for his kind suggestions regarding computer programming. This work was partially supported by a Grant-in-Aid for Scientific Research from the Japanese Ministry of Education, Science and Culture, which the authors wish to thank. This paper is based on part of the Ph.D. thesis of one of authors (E.Y.) presented to Hokkaido University, 1989.

[1]A. Yamashita, Kisho Kenkyu Note, Meteorol. Soc. Jpn. **123**, 47 (1974) (in Japanese).
[2]T. Gonda and T. Yamazaki, J. Cryst. Growth **45**, 66 (1978).
[3]T. Kuroda, J. Cryst. Growth **65**, 27 (1983).
[4]T. Kobayashi and T. Kuroda, *Morphology of Crystals , Part B,* edited by I. Sunagawa (Terra Scientific, Tokyo, 1987), p. 649.
[5]U. Nakaya, *Compendium of Meteorology,* edited by T. F. Malone (American Meteorological Society, Boston, 1951), p. 207; *Snow Crystals—Natural and Artificial* (Harvard Univeristy Press, Cambridge, MA, 1954).
[6]H. J. Aufm Kampe, H. K. Weickmann, and J. J. Kelly, J. Meteorol. **8**, 168 (1951).
[7]J. Hallett and B. J. Mason, Proc. R. Soc. London, Ser. A **247**, 440 (1958).
[8]T. Kobayashi, Philos. Mag. **6**, 1363 (1961).
[9]T. Kuroda and R. Lacmann, J. Cryst. Growth **56**, 189 (1982).
[10]Y. Furukawa, M. Yamamoto, and T. Kuroda, J. Cryst. Growth. **82**, 665 (1987).
[11]A. A. Chernov, J. Cryst. Growth **24/25**, 11 (1974).
[12]T. Kuroda, T. Irisawa, and A. Ookawa, J. Cryst. Growth **42**, 41 (1977).
[13]W. W. Mullins and R. F. Sekerka, J. Appl. Phys. **34**, 323 (1963).
[14]J. S. Langer, Rev. Mod. Phys. **52**, 1 (1980).
[15]K. Isono, M. Komabayasi, and A. Ono, J. Meteorol. Soc. Jpn. **35**, 327 (1957).
[16]T. Gonda and M. Komabayasi, J. Meteorol. Soc. Jpn. **48**, 440 (1970); **49**, 32 (1971).
[17]T. Gonda, J. Meterol. Soc. Jpn. **54**, 233 (1976).
[18]T. Gonda, J. Cryst. Growth **49**, 173 (1980).
[19]R. C. Brower, D. A. Kessler, J. Koplik, and H. Levine, Phys. Rev. Lett. **51**, 1111 (1983); Phys. Rev. A **29**, 1335 (1984).
[20]E. Ben-Jacob, N. Goldenfeld, J. S. Langer, and G. Schön, Phys. Rev. A **29**, 330 (1984).
[21]J. Nittmann and H. E. Stanley, Nature (London) **321**, 663 (1986); J. Phys. A **20**, L1185 (1987).
[22]F. Family, D. E. Platt, and T. Vicsek, J. Phys. A **20**, L1177 (1987).
[23]E. Yokoyama and T. Kuroda, *Dynamics of Ordering Processes in Condensed Matter,* edited by S. Komura and H. Furukawa (Plenum, New York, 1988), p. 95.
[24]T. A. Witten and L. M. Sander, Phys. Rev. B **27**, 5686 (1983).
[25]R. Xiao, J. I. D. Alexander, and F. Rosenberger, Phys. Rev. A **38**, 2447 (1988).
[26]M. Komabayasi, J. Rech. Atmos. **6**, 307 (1972).
[27]D. A. Kessler, J. Koplik, and H. Levine, Phys. Rev. A **30**, 2820 (1984).
[28]Y. Saito, G. Goldbeck-Wood, and H. Müller-Krumbhaar, Phys. Rev. Lett. **58**, 1541 (1987).
[29]T. Kuroda, J. Meteorol. Soc. Jpn. **62**, 552 (1984).
[30]E. Yokoyama and T. Kuroda, J. Meteorol. Soc. Jpn. **66**, 927 (1988).
[31]W. B. Burton, N. Cabrera, and F. C. Frank, Philos. Trans. R. Soc. London, Ser. A **243**, 299 (1951).
[32]N. Cabrera and M. M. Levine, Philos. Mag. **1**, 450 (1956).
[33]E. Yokoyama, Ph.D. thesis, Department of Geophysics, Hokkaido University, 1989.
[34]T. Sei and T. Gonda, J. Cryst. Growth **94**, 697 (1989).
[35]W. B. Hillig, Acta. Metall. **14**, 1868 (1966).
[36]J. Kiefer and B. N. Hole, J. Chem. Phys. **7**, 3206 (1977).
[37]W. Beckmann and R. Lacmann, J. Cryst. Growth **58**, 443 (1982).
[38]T. Kuroda and T. Gonda, J. Meteorol. Soc. Jpn. **62**, 563 (1984).
[39]A. Seeger, Philos. Mag. **44**, 1 (1953).
[40]T. Kuroda, J. Cryst. Growth **71**, 84 (1985).
[41]E. Yokoyama and T. Kuroda, J. Phys. (Colloq.) **47**, C1-347 (1987).

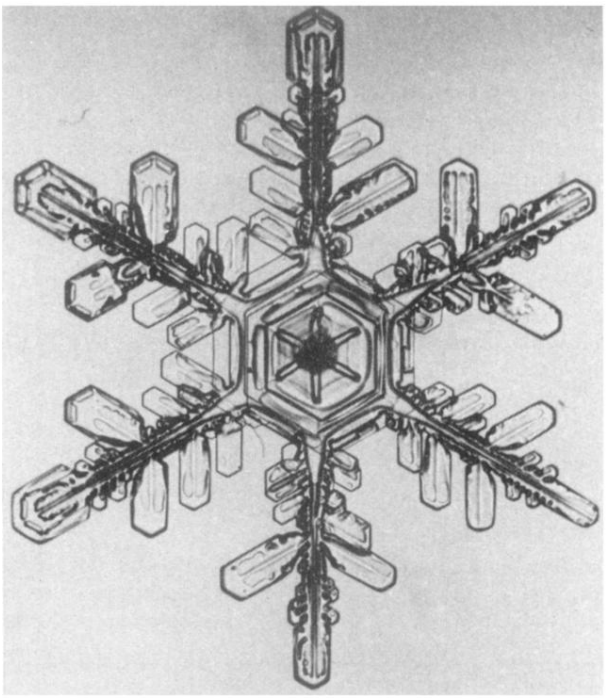

FIG. 2. A typical example of snow crystals (provided by Furukawa).